energies

MDPI

Article

Generation and Propagation Characteristics of an Auto-Ignition Flame Kernel Caused by the Oblique Shock in a Supersonic Flow Regime

Wenxiong Xi [1], Mengyao Xu [1], Chaoyang Liu [2], Jian Liu [1,*] and Bengt Sunden [1,3]

[1] School of Aeronautics and Astronautics, Central South University, Changsha 410012, China; 13739076081@163.com (W.X.); 15130715317@163.com (M.X.); bengt.sunden@energy.lth.se (B.S.)
[2] College of Aerospace Science and Engineering, National University of Defense Technology, Changsha 410015, China; liuchaoyang08@nudt.edu.cn
[3] Department of Energy Sciences, Lund University, P.O. Box 118, SE-22100 Lund, Sweden
* Correspondence: jian.liu@csu.edu.cn

Abstract: The auto-ignition caused by oblique shocks was investigated experimentally in a supersonic flow regime, with the incoming flow at a Mach number of 2.5. The transient characteristics of the auto-ignition caused by shock evolvements were recorded with a schlieren photography system, and the initial flame kernel generation and subsequent propagation were recorded using a high-speed camera. The fuel mixing characteristics were captured using NPLS (nanoparticle-based planar laser scattering method). This work aimed to reveal the flame spread mechanism in a supersonic flow regime. The effects of airflow total temperature, fuel injection pressure, and cavity length in the process of auto-ignition and on the auto-ignitable boundary were investigated and analyzed. From this work, it was found that the initial occurrence of auto-ignition is first induced by oblique shocks and then propagated upstream to the recirculation region, to establish a sustained flame. The auto-ignition performance can be improved by increasing the injection pressure and airflow total temperature. In addition, a cavity with a long length has benefits in controlling the flame spread from the induced state to a sustained state. The low-speed recirculating region created in the cavity is beneficial for the flame spread, which has the function of flame-holding and prevents the flame from being blown away.

Keywords: auto-ignition; supersonic flow; initial flame kernel; oblique shock; recirculating region

Citation: Xi, W.; Xu, M.; Liu, C.; Liu, J.; Sunden, B. Generation and Propagation Characteristics of an Auto-Ignition Flame Kernel Caused by the Oblique Shock in a Supersonic Flow Regime. *Energies* **2022**, *15*, 3356. https://doi.org/10.3390/en15093356

Academic Editor: Andrey Starikovskiy

Received: 7 April 2022
Accepted: 3 May 2022
Published: 5 May 2022

1. Introduction

Ignition and flame-holding are important issues in aircraft engine applications such as gas turbine combustors, ramjets, and scramjets. In these high-speed flow fields, the principle of combustion organization is to maintain a velocity equivalency relationship between the incoming reactant mixture and upstream flame propagation. The traditional flame propagation theory mainly concentrates on explaining the mechanism of flame-holding [1,2]. However, for a scramjet, the auto-ignition occurs when the air flow temperature increases to a threshold during the process of cruise flight. Fuel auto-ignition plays an important role in the process of velocity balance between the incoming reactant mixture and upstream flame propagation [3,4], which greatly affects the performance of the engine.

As a fundamental problem in combustion, auto-ignition phenomena have generally been investigated under various flow conditions in the past years [5,6]. Numerical calculations were used by different researchers to describe flame behaviors [7–9]. The chemical kinetics of auto-ignition, ignition delay time, and key mechanism were studied using shock tubes with engine-like conditions [10–12]. Meanwhile, the auto-ignition behavior within high temperature air is generally investigated using classical and simplified experimental facilities, such as a co-flow jet flame [13–15] and counter-flow flame [16,17]. In these studies, the kinetic-controlled auto-ignition phenomena are described in view of laminar and diffusion flames. However, the supersonic flow characteristics in scramjets, such as shock waves, have not been well considered, and the effect of shock waves on auto-ignition has been ignored. Recently, a more scramjet-like experimental condition was tested, and the flame structure in the crossflow of the heated air was observed, to analyze the behavior of auto-ignition and lift-off in a subsonic flow [18,19]. The results showed the process of auto-ignition for sustained flames in a high-temperature condition. However, how the auto-ignition and flame holding functions in the supersonic flow regime is still an unresolved problem.

The complexity of ignition and flame-holding in a supersonic flow-field is caused by the introduction of additional flow phenomena, such as shock waves, a strong shear layer, unstable wall boundary, and flow recirculation [20–22]. Although ignition and flame-holding have been investigated by some researchers, the mechanism based on the quasi-steady assumption of combustion is not available for the ignition transient, because of the interference between the shock and the flame. During the ignition transient, the generation of a shock wave has obvious influences on the combustion heat release and pressure increase downstream. The shock wave induced by combustion can change the fuel distribution from the initial cold condition and stationary combustion condition. Thus, the results obtained with a cold flow and stable combustion cannot be simply applied to common ignition dynamics [23–25]. Meanwhile, a shock wave has been proven to play a key role in the process of changing from self-ignition, transition, and flame-holding. It is found that the transition to flame-holding is both mixing-limited and reaction-limited, because of the shock wave, which increases the Damköhler number Da significantly. When sustained combustion is established, the combustion mode transition from a ramjet to a scramjet still depends on the state of the shock train structure [26]. How to distinguish the flame connecting phenomena caused by the co-existence of high-speed core flows and low velocity recirculating flows remains a problem. The occurrence of the flame depends on the fuel injection, flame holding device, the state of incoming air, and combustor structures. Rasmussen [27] investigated the flame stabilization mechanism using laser-induced fluorescence of OH and CH2O within a free stream with Ma = 2.4. The effect of the arrangement of fuel injections on combustion was studied. They found that the placement of the fuel injector had significant effects on the flame-holding mechanisms in a directly-fueled cavity flame-holder.

However, information on auto-ignition flame spread in the supersonic flow regime, particularly the effect of recirculation and oblique shocks on flame kernel generation and propagation, has rarely been covered in detail. In the present work, the auto-ignition process of hydrogen and ethylene was investigated experimentally in a supersonic flow regime with incoming air at Mach = 2.5. First, the auto-ignitable boundary was sketched, based on numerous ignition tests under various air flow total temperatures and fuel injection pressures. Then, the process of the generation of an initial flame kernel and propagation was observed with a high-speed camera and a schlieren photography system. Finally, the effect of the length of the cavity on flame establishment and propagation is considered and the auto-ignition mechanism is discussed.

2. Experimental Approach

2.1. Experimental Facility

The auto-ignition experiments were conducted in a directly-connected supersonic combustion test facility, which was composed of an air heater, an isolator, a combustor, and an expanding sector. Figure 1 shows a schematic of the layout of the ignition test system. The mass flow rate in the supersonic combustor was 1 kg/s at Ma = 2.5, and the total pressure was 1.6 MPa. The incoming air was heated through a vitiated heater, in which ethanol, oxygen, and air were supplied to burn and accordingly generate heat. The entrance condition was set based on the typical cruise flight of a scramjet. The total temperature of the heated air could be changed by adjusting the heat release power in the vitiated heater. More details about the ignition facility are described in refs. [28,29].

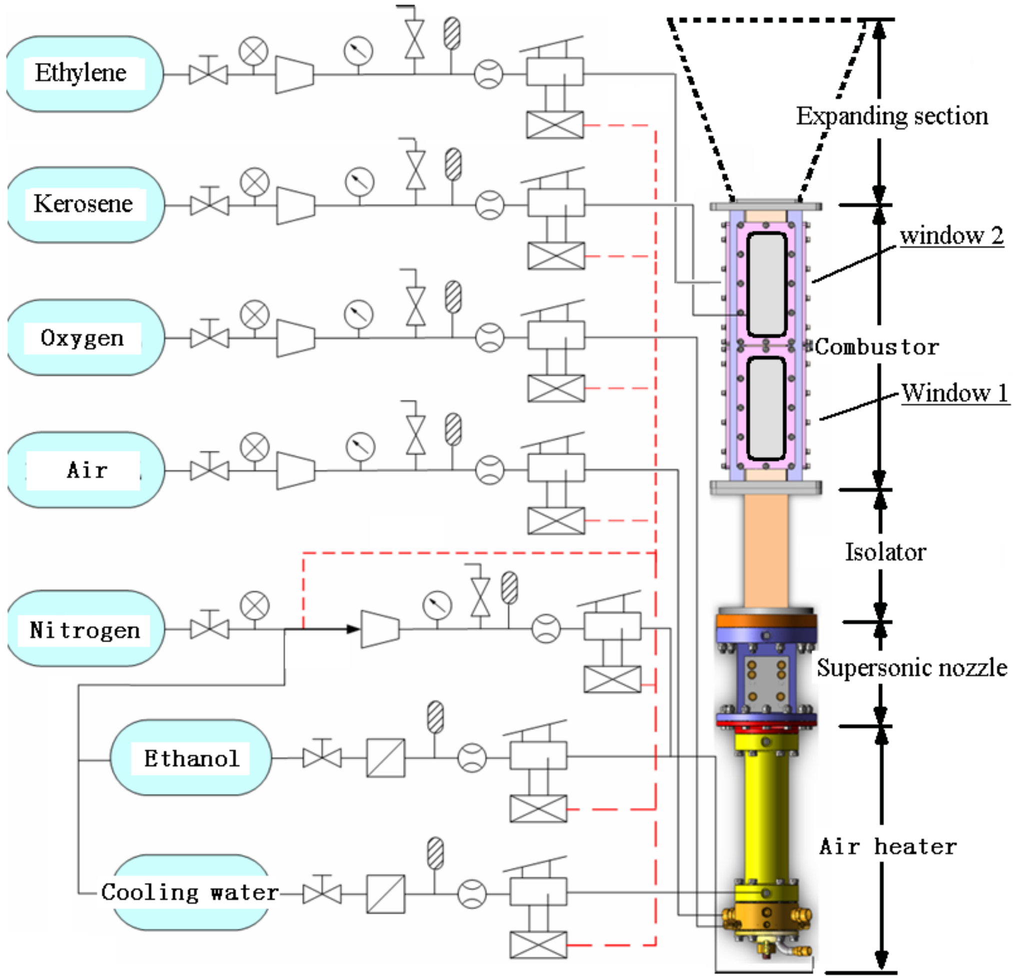

Figure 1. Schematic of the ignition system.

2.2. Combustor Configuration

Figure 2 shows a schematic diagram of the supersonic combustor for the auto-ignition test. The height of the straight combustor section was 40 mm, and the width was 50 mm. It was connected to an expanding section for exhaust gas. The cavity used for flame-holding had a depth of 8 mm. The cavity length could be changed from 24 mm to 56 mm, to investigate the effect of the cavity length. The cavities with different lengths were, respectively, named LD3, LD5, and LD7. Ethylene and hydrogen were used as the test fuel. The fuel was injected at sonic speed in a direction perpendicular to the air stream through a single hole with a diameter of 1 mm, located in the test section wall. The distance from the injection placement to the cavity was 30 mm. The fuel injection pressure could be adjusted from 1 MPa to 3.2 MPa, with a fuel stagnation temperature of 296 K. The total temperature of the incoming air was varied from 1400 K to 1650 K. Upstream of the cavity, at a distance of 60 mm, a pressure sensor was installed to measure the combustor pressure. To improve the auto-ignition performance of the fuel, a ramp with an inclination angle of 18 degrees was installed on the top wall to generate oblique shocks. Related geometric parameters and flow conditions are listed in Table 1.

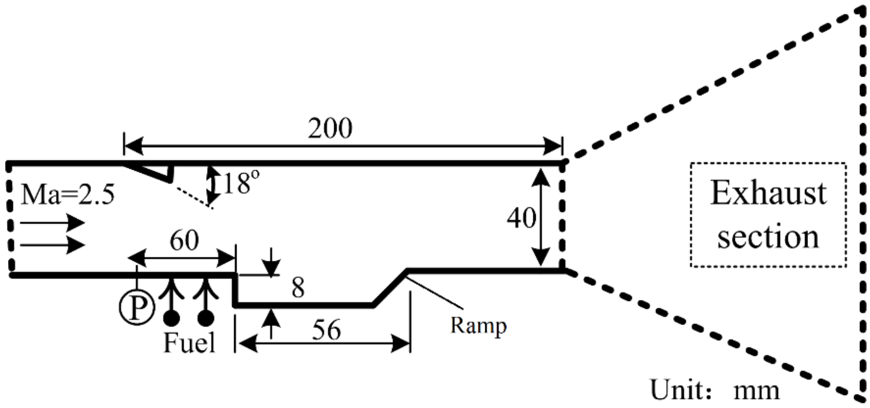

Figure 2. Schematic diagram of the supersonic combustor for the auto-ignition test.

Table 1. Related parameters of the supersonic combustor.

Related Parameters			
Mach number	2.5	Total temperature	1400–1650 K
Length of fuel injection	60 mm	Injection pressure	1.0–3.2 Mpa
Length of cavity	24–56 mm	Angle of oblique shock	18°
Depth of cavity	8 mm	Height of combustor	40 mm
Width of combustor	50 mm	Test length of combustor	200 mm

2.3. Method for Flow-Field and Flame Observation

Quartz windows were mounted on the side walls of the combustor, to enable optical measurements. Schlieren photography, as shown in Figure 3c, was performed using a high speed video system MotionBLITZ (Mikrotron GmbH, Unterschleißheim, Germany) and was used to record the shock train involution during the ignition transient. A 532-nm laser system was used as a back light source, to eliminate the interference of the flame emission. Images of the initial auto-ignition flame kernel and subsequent flame propagation were acquired with a Photron FASTCAM-SA5, as shown in Figure 3b. The camera system consisted of a vidicon, lens, and processor (Photron Limited, San Diego, CA, USA). The lens was a Nikon 50~500-mm zoom lens (Photron Limited San Diego, CA, USA). The image sensor was a CMOS with high sensitivity, and the frame rate could reach 120 thousand frames per second.

The mixing characteristics of the vertical fuel injection were displayed utilizing NPLS (nanoparticle-based planar laser scattering) technology. The NPLS measurement system consisted of a computer, synchronizer, CCD camera, and pulse laser, as shown in Figure 3d. In the NPLS measuring system, the computer controlled the interaction of the components and received the experimental images. The input and output parameters of the synchronizer were controlled by software, and the related assisting-computers were controlled by the signal of the synchronizer. Time diagrams of the CCD exposure and laser output of the pulse laser were adjusted for the purpose of measurement. The laser beam was transformed into a sheet using a cylindrical lens. In the experiment, the thickness of the laser sheet was 1 mm. The synchronizer had eight output ports, with a time accuracy of 0.25 ns. The CCD camera was an interline transfer type CCD, with a shortest frame time of 200 ns and array resolution of 2000 $\times$ 2000. The gray levels of each pixel were 4096, using a micro-lens. The pulsed laser light source was a double cavity Nd: YAG laser machine with an output laser wavelength of 532 nm, pulse duration time of 6 ns, and highest energy of a single pulse of 350 mJ.

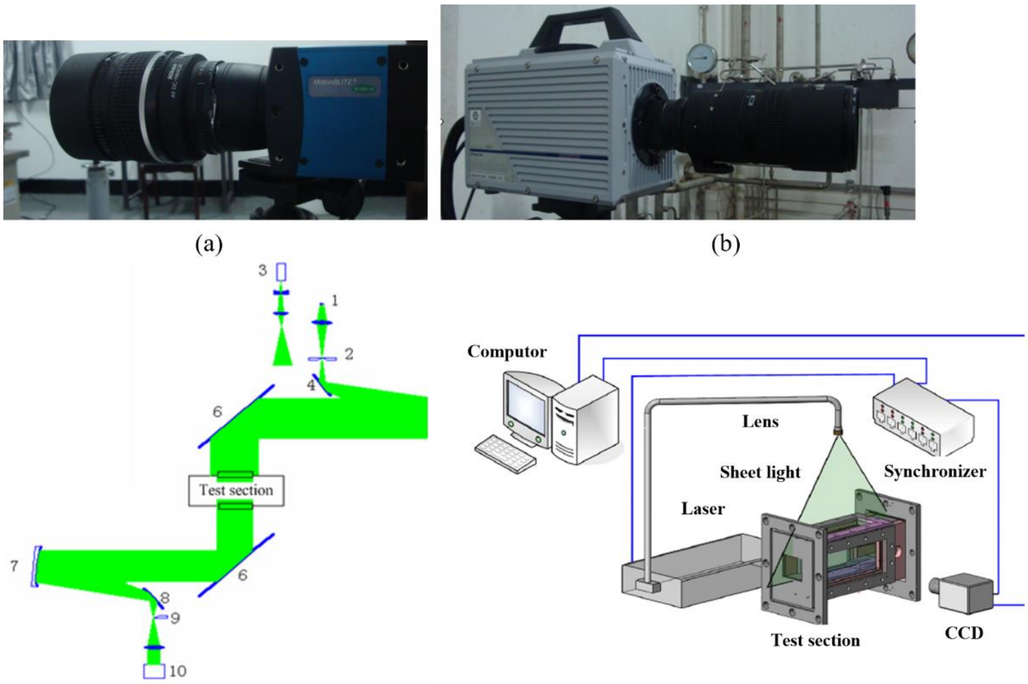

Figure 3. High speed image recording devices used for the ignition tests: (**a**) MotionBLITZ; (**b**) Photron FASTCAM-SA5; (**c**) set-up of the schlieren photography; (**d**) set-up of the test section and the NPLS system.

3. Results and Discussion

3.1. Results of Auto-Ignitable Boundary

In the current work, the occurrence of auto-ignition was captured from the light scattering images through the windows. The ignition process began with a well-established incoming flow condition with the air heater. Then the fuel injection switch was turned on, with a duration of 2 s, which is a sufficiently long time to reach a time-averaged non-premixed flow field. Auto-ignition took place, with the occurrence of an initial flame kernel. Based on the acquired sequential flame spread images, three cases of auto-ignition event could be classified: a failed case, without initial flame kernel generation; a case of auto-ignition kernel appearance, without a sustained flame; and a case of successful global ignition. To investigate the effect of the total temperature and injection, several ignition tests were performed, with a stepwise increase of temperature by 25 K and pressure by 0.5 MPa.

Figure 4 presents the experimental results of the auto-ignitable boundary under different injection pressures and total temperatures. The suitable auto-ignitable area is shown in the right corner of the figure. From the figure, it is evident that a higher total temperature of the incoming air and injection pressure improved the performance of auto-ignition. A high temperature reduced the auto-ignition delay time of the reactants, and a high injection pressure enhanced the fuel mixing and decreased the mixing time, to create an ignitable concentration condition. Overall, auto-ignition appeared in a temperature range of 1500 K–1650 K and injection pressure range of 2.0 MPa–3.5 MPa. From the experimental results, it can be seen that total temperature had a greater influence compared to the injection pressure. Auto-ignition could occur at a high total temperature of incoming air, even with a relatively low injection pressure. From the auto-ignitable boundary with a “C” shape, it is also evident that for a certain total temperature of incoming air, there exists an optimized injection pressure of fuel.

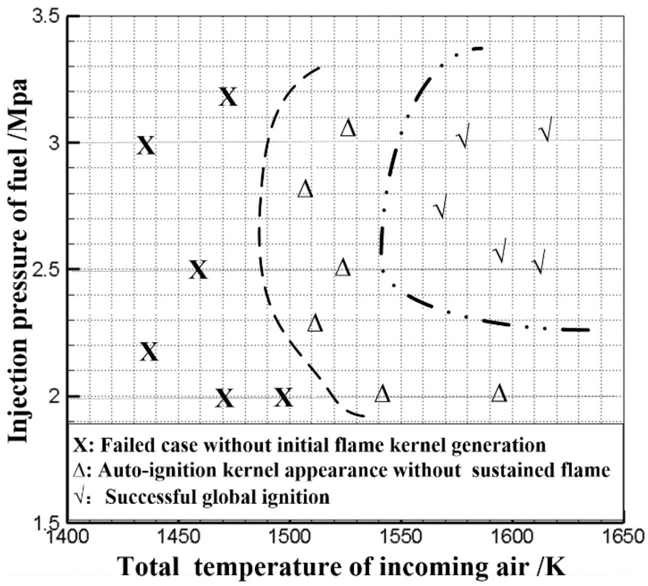

Figure 4. Experimental results of auto-ignitable boundary under different injection pressures of the ethylene and total temperatures of the incoming air.

3.2. Auto-Ignition Transient and Initial Flame Kernel Propagation

The laser schlieren system was employed to acquire the auto-ignition transient. Figure 5 presents typical sequential schlieren images of the ethylene auto-ignition and the shock wave evolvement of the auto-ignition. The total temperature of the incoming air was 1480 K and the injection pressure of the ethylene was 1.5 MPa. In Figure 5, the layout and interaction of shock waves are clearly displayed. The mixing of the fuel injection along the combustor can be approximately evaluated according to the faint contrast grade. It is noted that the boundary edge of fuel transportation has been manually marked with dash-dotted lines. Figure 5a shows the initial phase of the shock evolution. The time interval of the snapshots was 0.4 ms, with an exposure time of 50 μs. The subsequent quasi-stable phase of the establishment of the shock train is depicted in Figure 5b, with a time interval of 0.2 ms. The first image of Figure 5a displays the flow-field characteristics just before the emergence of auto-ignition. As shown in the photograph, several typical shocks are clearly observed: an oblique shock induced by the ramp, a bow shock by the fuel injection, the expanding shock of the ramp rear, and the intersection reflected by the shear layer. When the ignition begins, the intersection circled with dashed lines in the figure is pushed ahead, and then the shock train forms. The process of shock train generation was accompanied by a boundary separation caused by downstream heat release. Compared with the cold condition before ignition, the intensity of the fuel mixing in the state of stable combustion was enhanced due to the heat release. One reason for this is that the depth of fuel penetration was increased due to the decreased velocity of the main-flow. Another reason is that the turbulence induced by the shock train also improved the mixing of the reactants.

Figure 6 illustrates corresponding dynamic flame sequential images of the ethylene auto-ignition. The time interval of the snapshots was 83 μs. As shown in Figure 6, the process of flame propagation is divided into two phases: the initial flame kernel generation phase (left), and the quasi-stable flame phase (right), corresponding to Figure 5a,b. The first phase involved the initial flame generation and heat accumulation by the downstream strong combustion. The second phase refers to the upstream flame spread through the low speed circulation cavity and the establishment of a sustained flame.

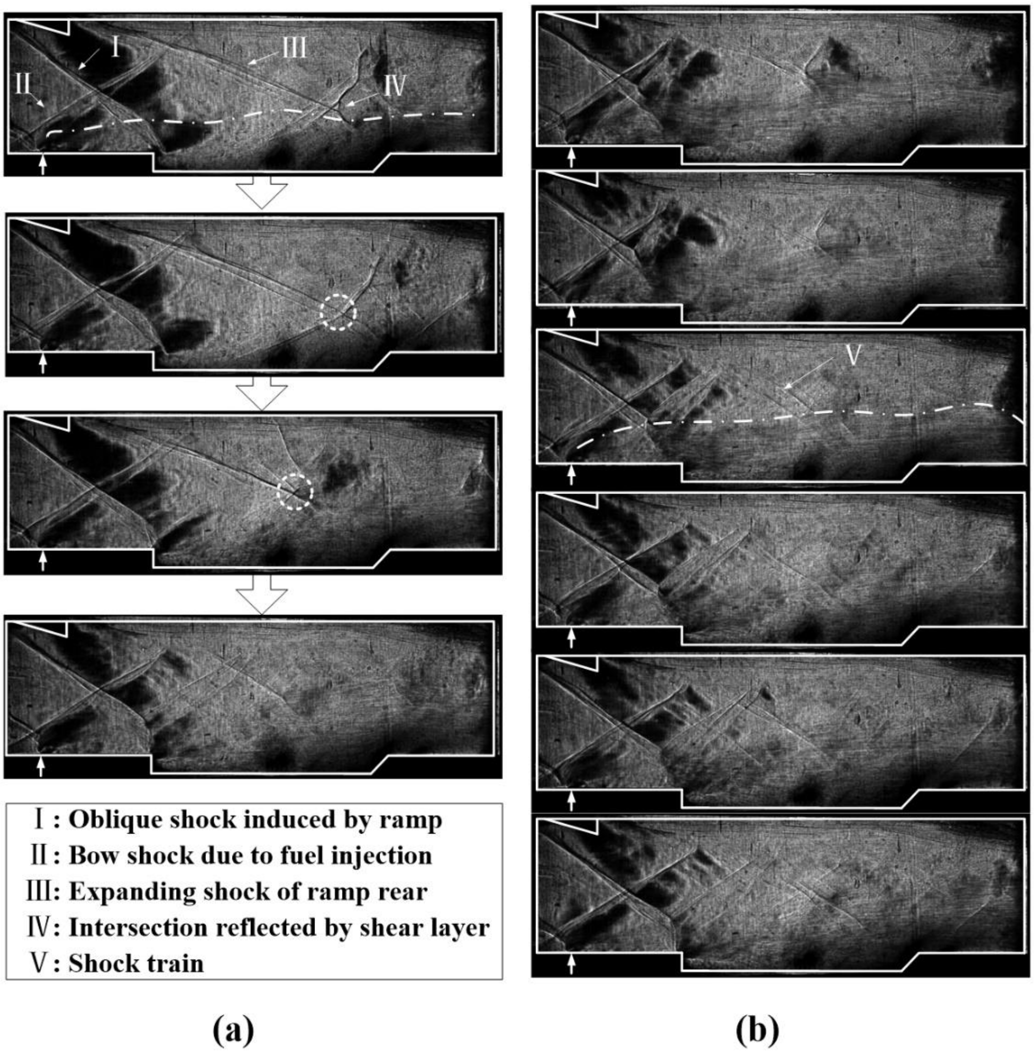

Figure 5. Sequential schlieren images of the ethylene auto-ignition: (**a**) initial phase of the shock evolution, with a time interval of 0.4 ms and an exposure time of 50 μs; (**b**) subsequent quasi-stable phase of the establishment of the shock train, with a time interval of 0.2 ms and an exposure time of 50 μs.

By analysis of the shock layout displayed in Figure 5, it was revealed that the initial flame kernel was caused by the incidence of the oblique shock on the ramp. The reason for this is that the auto-ignition delay time of the reactants was shortened due to the increased temperature and pressure behind the shock. The first visible auto-ignition kernel was at an angle relative to the core of the flow field just downstream of the cavity. The distance from the fuel injection point to the first visible flame kernel was defined as the ignition delayed distance $L_{ignition}$, with a length of 76 mm. Unlike the case of the combustion directly induced by the shock, this made the interaction between the flame and the shock uncoupled, with a relatively long delayed distance. The feedback of the ignition transition and flame propagation was caused by the downstream accumulation of heat release. The heat release made the pressure increase to the boundary separation, and then a shock train was formed. The effect of the formed shock train on the flame propagation is displayed in the seventh image of Figure 6, in which the edges of the flame were created by the shock train.

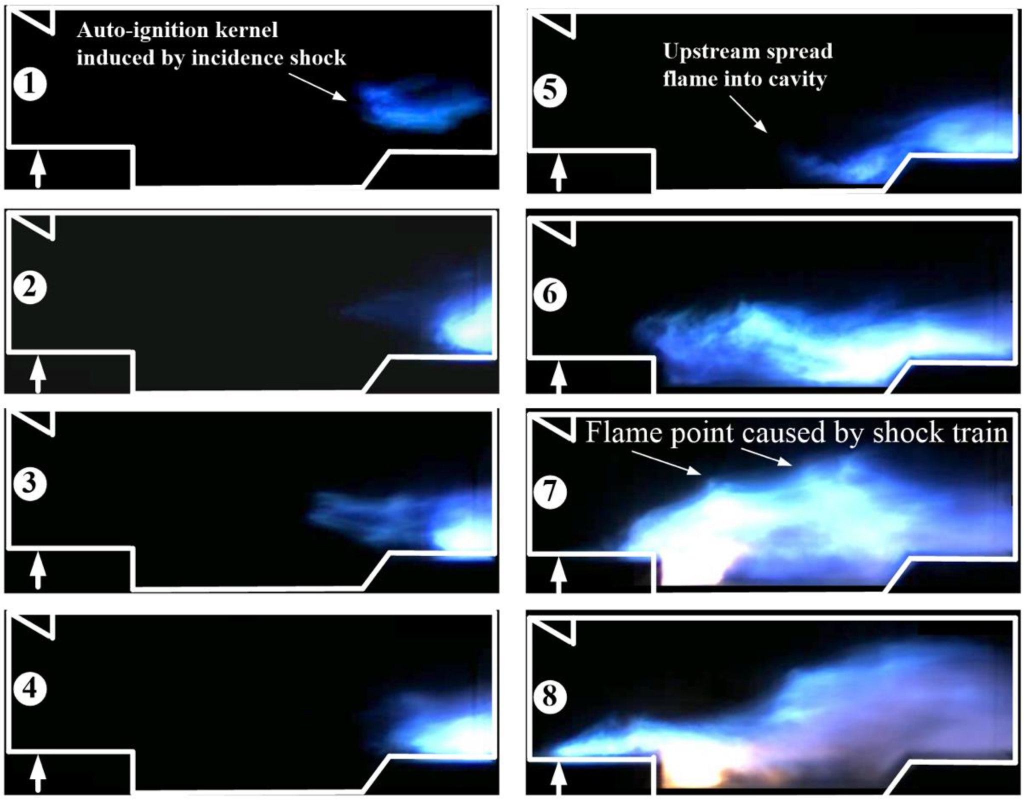

Figure 6. Dynamic flame sequential images of the ethylene auto-ignition, with a time interval of 83 µs.

3.3. Effect of the Cavity on Flame Stabilization and Propagation

To investigate the influence of the cavity on the establishment of a sustained auto-ignition flame, the generation and propagation of the ethylene auto-ignition flame without the cavity was measured as a baseline case. Dynamic and sequential flame images of the ignition are shown in Figure 7, in which the ramp was present to create an oblique shock. Similar to the case of Figure 6, the flame kernel was located at the core of the flow-field, with a certain ignition delay. The subsequent flame propagation followed the common flame spread routine through the separated boundary. The characteristics of the flame dynamics play an important role in this phenomenon. As shown in Figure 7, the flame shape changed abruptly and changed with a low frequency. The unsteadiness is also clearly evident from the pressure response in Figure 8.

Figure 8 shows the pressure response characteristics of the ethylene auto-ignition process. The pressure measured near the wall of the combustor is indicated by Pen, and it varied from 90 kPa to 150 kPa, with time intervals ranging from 115 ms to 296 ms. The total pressure of the main flow (P_c) measured in the air heater and the injection pressure of ethylene (P_{c2h4}) were almost constant during the auto-ignition period. Therefore, the unsteadiness of the airflow and the fuel supply system was not caused by the variation of the pressure response. It can be concluded that the shock generated by the ramp was the main factor behind the occurrence of the auto-ignition flame kernel, and the flow recirculation created by the cavity had benefits for the flame's upstream propagation and stabilization.

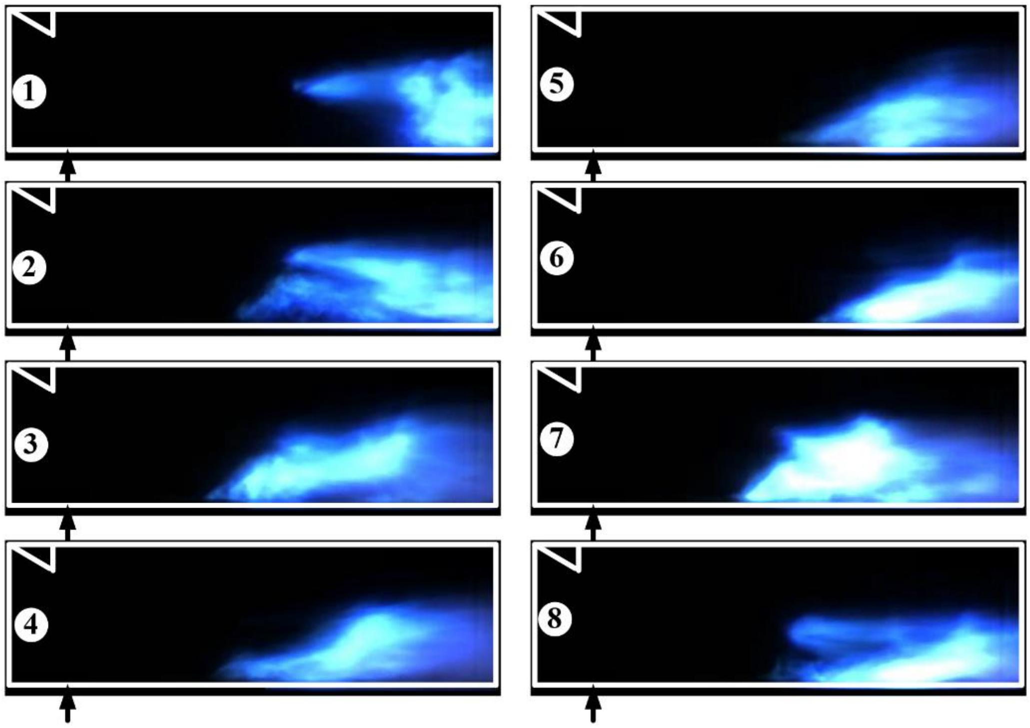

Figure 7. The dynamic flame images of the ethylene auto-ignition without the cavity (the image parameters are similar to Figure 5).

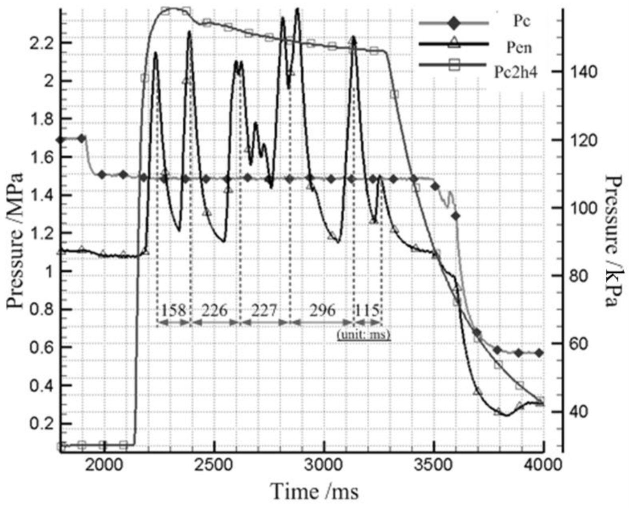

Figure 8. Pressure response characteristics of the ethylene auto-ignition process (P_c indicates pressure of the air heater; P_{en} indicates pressure measured in the supersonic combustor; P_{c2h4} indicates injection pressure of the ethylene).

To obtain more details about the effect of the cavity on flame propagation and stabilization, three types of cavities were tested and compared. Considering the ignition efficiency, hydrogen was selected as the test fuel. Compared with ethylene, the ignition delay time for hydrogen is shorter, with a fast flame spread velocity in the same conditions. Owing to the weak radiation of the hydrogen flame, heated air was seeded with nanoparticles of SiO2 (silicon dioxide) to intensify the flame visibility, which provided benefits in acquiring photographs with a much shorter exposure time and higher acquisition speed, for capturing the instantaneous flame dynamics. Figure 9 presents the initial flame kernel evolvement of the hydrogen auto-ignition. Three types of cavities were compared, with various cavity lengths, i.e., LD7, LD5, and LD3. The injection pressure was set as 2.5 MPa. As depicted in Figure 9, the characteristics of flame generation and propagation were similar to the case described above. The length of the cavity had no obvious influence on the location of the occurrence of the flame kernel. Thus, the delayed residence time of the reactant by the cavity was not the main mechanism behind the first occurrence of auto-ignition. In addition, the extended recirculation zone with a longer cavity is beneficial for the initial heat release accumulation during the flame upstream propagation. The LD7 cavity had the strongest heat release, with an intensive light emission; while the flame of the shorter cavity tended to be blown away.

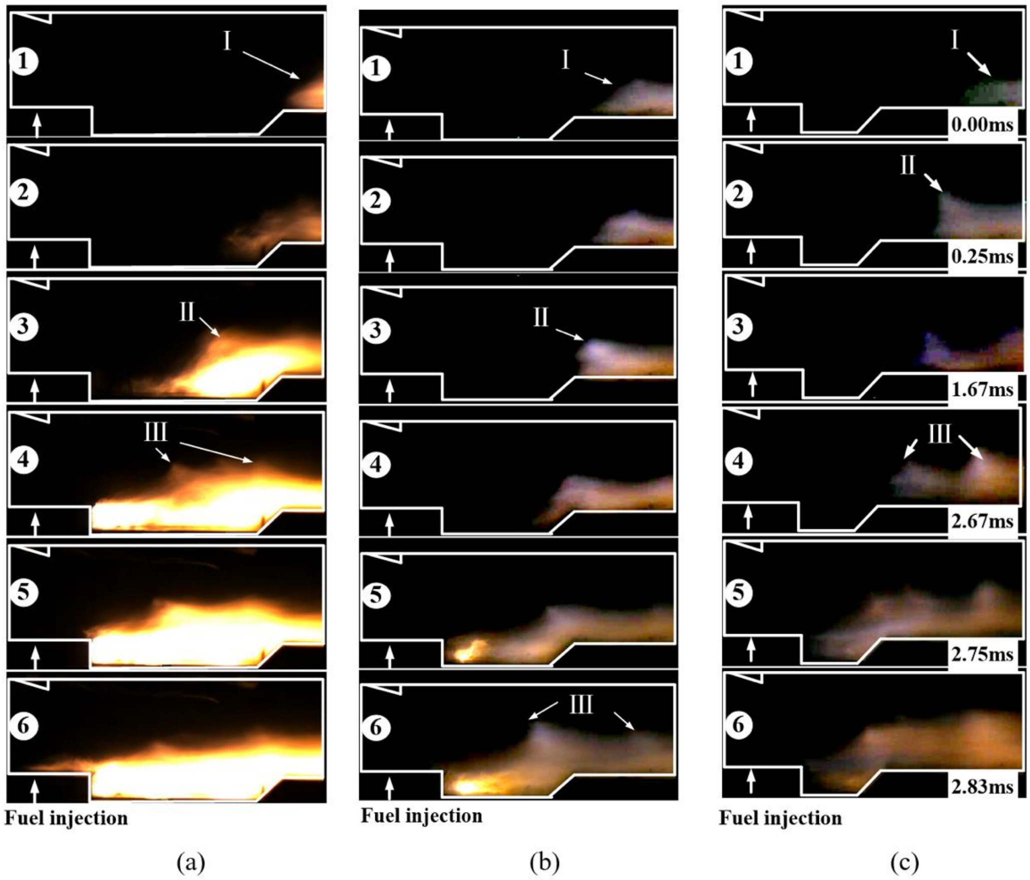

Figure 9. Initial flame kernel evolvement of the hydrogen auto-ignition with various cavity lengths: (**a**) case of LD7 cavity; (**b**) case of LD5 cavity; (**c**) case of LD3 cavity (the exposure times were all set as 83 μs, with a frame speed of 12,000 f/s, except for (**c**), whose time intervals are marked on the images; I indicates the occurrence of the initial flame; II indicates the flame position induced by the incidence shock; III indicates the flame point caused by the shock train).

3.4. Fuel Distribution Based on NPLS Method

Figure 10 shows the mixing characteristics of the fuel injection observed using NPLS when a steady flame was established. The nanoparticle generator was driven by high-pressure gaseous ethylene. When the flow field was measured with NPLS, the nanoparticles were injected into, and mixed with, the inflow of the flow field. When the flow was established in the observation window, the synchronizer controlled the laser pulse and the CCD camera, to ensure synchronization of the emissions scattered by nanoparticles and the exposure of the CCD. The scattering image gave a clear fuel distribution boundary, in which the fuel penetration depth was influenced by the injection pressure. Combined with the flame image obtained above, this shows that a delay in the distance existed for the mixing between the fuel and the incoming air. The front flame edge could propagate upstream along a suitable concentration boundary, until a steady flame was formed.

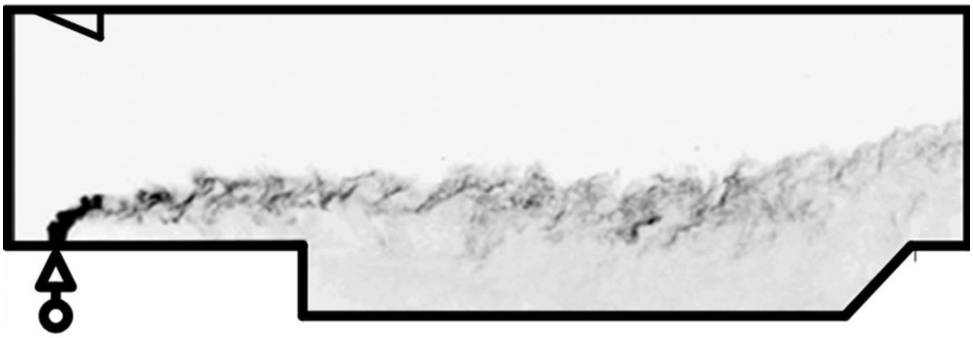

Figure 10. Mixing characteristic of fuel injection observed using NPLS.

3.5. Analysis of Auto-Ignition and the Flame Spread Mechanism

Based on the aforementioned analysis, a fundamental physical description of the occurrence of auto-ignition and flame propagation can be summarized. The auto-ignition process with a cross-flow effect is shown in Figure 11. After the initial flame kernel was formed, it was divided into two parts and transported downstream. One part was further mixed and burned with the mainstream flame kernel that had not completed self-ignition and accumulated heat, which is represented by propagation path 1. The other part underwent mixing combustion in the low-speed region in the boundary layer, represented by propagation path 2. When the combustion heat release caused boundary layer separation, a boundary layer countercurrent flame appeared. At this time, the flame propagation path 3 spread upstream along the equivalent of the chemically appropriate equivalent ratio, presenting the characteristics of a "three-bifurcation flame", which is stable at a special position. For a successful auto-ignition event, there are three sub-processes required: the mixing process, induction process, and thermal runaway process. The mixing process, similarly to the preparation process, includes fuel injection and transport downstream without chemical reactions. The distance for forming a suitable concentration condition is defined as the mixing length indicated by L_{mix}. Subsequently, the distance of the induction process is named the induction length (L_{induce}), in which the primary reaction process starts, together with the accumulation of the auto-ignition precursor formaldehyde (CHO). The existence of an induction length makes the flame front invisible. The subsequent thermal runaway process is characterized by a massive heat release, accompanied with a visible light scattering of OH radiation. The following two sub-processes are recognized as distributed auto-ignition reactions and disturbed reaction layers from the perspective of stationary flame structures [18]. At the ignition transient, a complete flame spread involves the downstream convective and diffusive flame, and the upstream boundary flame.

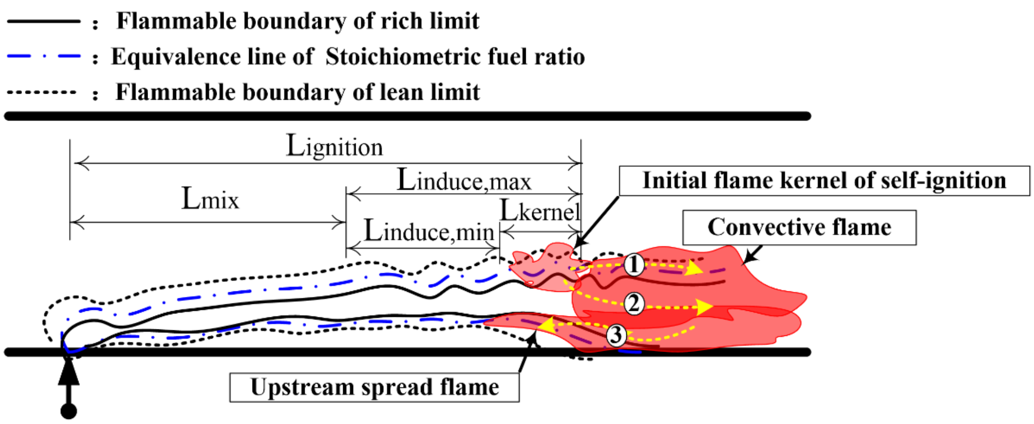

Figure 11. Schematic diagram of auto-ignition with cross-flow injection.

Figure 12 explains the occurrence of flame auto-ignition and the spread mechanism in a supersonic flow with the placement of the ramp and the cavity. From the figure, it is seen that 4, 5, 6, and 7 are developments of path 3; i.e., upstream spread flame in the ramp and the cavity. While, 4 and 5 are the upstream spread flame in the cavity, 6 is the trapped flame with flow circulation and 7 is the downstream spread flame in the cavity. In Figure 12, the incidence of the shock can reduce the mixing length and the induction length. Thus, the induction reaction is brought forward. When the initial flame kernel is generated, the downstream flame development is similar to the case mentioned above in Figure 11. It is necessary to span an additional distance for the combustion process, shown as L_{spread}. The role of the cavity is to reduce the L_{spread} and ensure upstream propagation, until the trapped circulation flame is established. A cavity with a long length has benefits for the flame transition from the induced state to a sustained state.

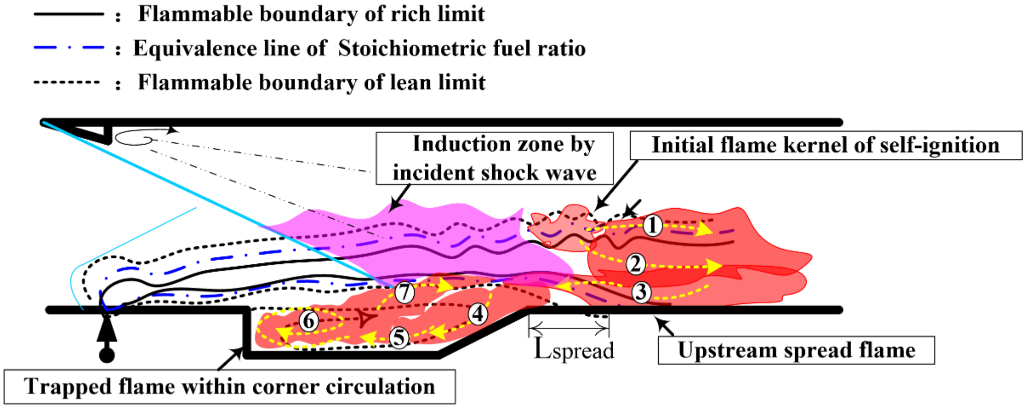

Figure 12. Schematic diagram of an auto-ignition flame and spread mechanism, with the effects of the ramp and the cavity.

4. Conclusions

In the present work, auto-ignition of ethylene and hydrogen caused by an oblique shock was investigated experimentally in a supersonic flow regime, with incoming air at Mach = 2.5. The auto-ignition transient was observed using a schlieren photography system, and the process of the occurrence of the flame kernel and its subsequent propagation was acquired using a high-speed camera. The effects of the incoming airflow total temperature, fuel injection pressure, and length of the cavity on the auto-ignition and auto-ignitable boundary were considered and compared. Several conclusions were drawn, as follows:

(1) The auto-ignition performance was extended by increasing the injection pressure and total temperature of the airflow, with enhanced mixing efficiency and decreased ignition delay time.
(2) The flame evolvement was described as follows: the occurrence of auto-ignition is induced by oblique shocks and then propagates upstream to the recirculating region. Finally, a sustained flame is established inside the recirculating region.
(3) A cavity with a long length has benefits for the flame transition from the induced state to a sustained state. Meanwhile, the low speed recirculation created in the cavity has benefits for the flame spread, with the function of preventing the flame from being blown away by flow oscillations.

Author Contributions: Conceptualization, W.X. and J.L.; methodology, W.X.; software, M.X.; validation, W.X., J.L. and C.L.; investigation, W.X.; writing—original draft preparation, J.L.; writing—review and editing, B.S.; supervision, C.L.; funding acquisition, W.X. All authors have read and agreed to the published version of the manuscript.

Funding: This work was supported by the National Natural Science Foundation of China (Grant No. 51606220).

Conflicts of Interest: The authors declare no conflict of interest.

Nomenclature and Abbreviations

Latin characters	
Da	Damköhler number
$L_{ignition}$	ignition delayed distance
L_{induce}	induction length
L_{mix}	mixing length
L_{spread}	flame spread length
Ma	Mach number
P_{en}	pressure in the combustion chamber
P_c	total pressure of the air flow
P_{c2h4}	injection pressure of the ethylene
Abbreviations	
CCD	charge coupled device
CMOS	complementary metal oxide semiconductor
NPLS	nanoparticle-based planar laser scattering

References

1. Chung, S.H. Stabilization, propagation and instability of tribrachial triple flames. *Proc. Combust. Inst.* **2007**, *31*, 877–892. [CrossRef]
2. Buckmaster, J. Edge-flames. *Prog. Energy Combust. Sci.* **2002**, *28*, 435–475. [CrossRef]
3. Gordon, R.L.; Masri, A.R.; Pope, S.B.; Goldin, G.M. Transport budgets in turbulent lifted flames of methane autoigniting in a vitiated co-flow. *Combust. Flame* **2007**, *151*, 495–511. [CrossRef]
4. Liu, C.; Zhang, J.; Jia, D.; Li, P. Experimental and numerical investigation of the transition progress of strut-induced wakes in the supersonic flows. *Aerosp. Sci. Technol.* **2021**, *120*, 107256. [CrossRef]
5. Mastorakos, E. Ignition of turbulent non-premixed flames. *Prog. Energy Combust. Sci.* **2009**, *35*, 57–97. [CrossRef]
6. An, B.; Sun, M.; Wang, Z.; Chen, J. Flame stabilization enhancement in a strut-based supersonic combustor by shock wave generators. *Aerosp. Sci. Technol.* **2020**, *104*, 105942. [CrossRef]
7. Jones, W.P.; Navarro-Martinez, S. Numerical study of n-Heptane auto-ignition using LES-PDF methods. *Flow Turbul. Combust.* **2009**, *83*, 407–423. [CrossRef]
8. Jones, W.P.; Navarro-Martinez, S.; Rohl, O. Large eddy simulation of hydrogen auto-ignition with a probability density function method. *Proc. Combust. Inst.* **2007**, *31*, 1765–1771. [CrossRef]
9. Richardson, E.S.; Yoo, C.S.; Chen, J.H. Analysis of second-order conditional moment closure applied to an auto-ignitive lifted hydrogen jet flame. *Proc. Combust. Inst.* **2009**, *32*, 1695–1703. [CrossRef]
10. Gokulakrishnan1, P.; Gaines, G.; Klassen, M.S. Autoignition of Aviation Fuels: Experimental and Modeling Study. In Proceedings of the 43rd AIAA/ASME/SAE/ASEE Joint Propulsion Conference & Exhibit, Cincinnati, OH, USA, 8–11 July 2007.
11. Dean, A.J.; Penyazkov, O.G.; Sevruk, K.L.; Varatharajan, B. Autoignition of surrogate fuels at elevated temperatures and pressures. *Proc. Combust. Inst.* **2007**, *31*, 2481–2488. [CrossRef]
12. Athithan, A.A.; Jeyakumar, S.; Sczygiol, N.; Urbanski, M.; Hariharasudan, A. The Combustion Characteristics of Double Ramps in a Strut-Based Scramjet Combustor. *Energies* **2021**, *14*, 831. [CrossRef]
13. Medwell, P.R.; Kalt, P.A.M.; Dally, B.B. Imaging of diluted turbulent ethylene flames stabilized on a Jet in Hot Coflow (JHC) burner. *Combust. Flame* **2008**, *152*, 100–113. [CrossRef]
14. Oldenhof, E.; Tummers, M.J.; van Veen, E.H.; Roekaerts, D.J. Ignition kernel formation and lift-off behaviour of jet-in-hot-coflow flames. *Combust. Flame* **2010**, *157*, 1167–1178. [CrossRef]
15. Kaiser, S.A.; Frank, J.H. Spatial scales of extinction and dissipation in the near field of non-premixed turbulent jet flames. *Proc. Combust. Inst.* **2009**, *32*, 1639–1646. [CrossRef]
16. Pellett, G.L.; Vaden, S.N.; Wilson, L.G. Opposed Jet Burner Extinction Limits: Simple Mixed Hydrocarbon Scramjet Fuels vs. Air. In Proceedings of the 43rd AIAA/ASME/SAE/ASEE Joint Propulsion Conference & Exhibit, Cincinnati, OH, USA, 8–11 July 2007.
17. Ruan, C.; Chen, F.E.; Yu, T.; Cai, W.W.; Li, X.L.; Lu, X.C. Experimental study on flame/flow dynamics in a multi-nozzle gas turbine model combustor under thermo-acoustically unstable condition with different swirler configurations. *Aerosp. Sci. Technol.* **2020**, *98*, 11. [CrossRef]
18. Micka, D.J.; Driscoll, J.F. Stratified jet flames in a heated (1390 K) air cross-flow with autoignition. *Combust. Flame* **2012**, *159*, 1205–1214. [CrossRef]
19. Kurdyumov, V.; Fernandez-Tarrazo, E.; Linan, A. The anchoring of gaseous jet diffusion flames in stagnant air. *Aerosp. Sci. Technol.* **2002**, *6*, 507–516. [CrossRef]
20. Masuya, G.; Choi, B.; Ichikawa, N. Mixing and combustion of fuel jet in pseudo-shock waves. In Proceedings of the 40th AIAA Aerospace Sciences Meeting & Exhibit, Reno, NV, USA, 14–17 January 2002.
21. Mai, T.; Sakimitsu, Y.; Nakamura, H.; Ogami, Y.; Kudo, T.; Kobayashi, H. Effect of the incident shock wave interacting with transversal jet flow on the mixing and combustion. *Proc. Combust. Inst.* **2011**, *33*, 2335–2342. [CrossRef]

22. Li, F.; Sun, M.; Cai, Z.; Chen, Y.; Sun, Y.; Li, F.; Zhu, J. Effects of additional cavity floor injection on the ignition and combustion processes in a Mach 2 supersonic flow. *Energies* **2020**, *13*, 4801. [CrossRef]
23. Tetsuo, H.; Kan, K.; Sadatake, T.; Izumikawa, M.; Watanabe, S. Gas-sampling survey from exhaust flows in scramjet engines at Mach-6 flight condition. In Proceedings of the 40th AIAA/ASME/SAE/ASEE Joint Propulsion Conference and Exhibit, Fort Lauderdale, FL, USA, 11–14 July 2004.
24. Dai, J.; Cai, G.B.; Zhang, Y.; Yu, N.J. Experimental and numerical investigation of combustion characteristics on GO2/GH2 shear coaxial injector. *Aerosp. Sci. Technol.* **2018**, *77*, 725–732. [CrossRef]
25. Jeong, E.; O'Byrne, S.; Jeung, I.S.; Houwing, A.F.P. The effect of fuel injection location on supersonic hydrogen combustion in a cavity-based model scramjet combustor. *Energies* **2020**, *13*, 193. [CrossRef]
26. Fotia, M.L.; Driscoll, J.F. Ram-Scram Transition and Flame/Shock-Train Interactions in a Model Scramjet Experiment. *J. Propuls. Power* **2013**, *29*, 261–273. [CrossRef]
27. Rasmussen, C.C.; Dhanuka, S.K.; Driscoll, J.F. Visualization of flameholding mechanisms in a supersonic combustor using PLIF. *Proc. Combust. Inst.* **2007**, *31*, 2505–2512. [CrossRef]
28. Xi, W.X.; Wang, Z.G.; Li, Q.; Liang, J.H. Forced ignition of kerosene spray in supersonic flowfield with hot gas injection. *J. Aerosp. Power* **2012**, *27*, 2436–2441.
29. Xi, W.X.; Wang, Z.G.; Sun, M.B.; Liu, W.D.; Li, Q. Experimental investigation of ignition transient phase in model supersonic combustor. *J. Aerosp. Eng.* **2014**, *27*, 04014009.